Engineering Structures 104 (2015) 107–115

Contents lists available at ScienceDirect

Engineering Structures

journal homepage: www.elsevier.com/locate/engstruct



# Blast loading influence on load carrying capacity of I-column

Lukasz Mazurkiewicz *, Jerzy Malachowski, Pawel Baranowski

*Department of Mechanics and Applied Computer Science, Military University of Technology, 2 Gen. Sylwestra Kaliskiego Street, 00-908 Warsaw, Poland*

ARTICLE INFO

*Article history:*
Received 13 March 2015
Revised 15 September 2015
Accepted 22 September 2015

*Keywords:*
Load carrying capacity
Blast loading
FE analysis
Fluid structure interaction
Dynamic behaviour

ABSTRACT

The paper presents the multistage numerical analyses procedure for a load carrying capacity assessment of a blast loaded I-column. The procedure determines the ultimate axial load in four stages: static preload, dynamic blast loading, dynamic response after blast loading and a static load carrying capacity assessment of a deformed structure. Preload and assessment of the ultimate axial load were performed using static Newton–Raphson algorithm. Consequently, two dynamic cases were analysed using a commercial code with an explicit integration procedure (central difference method), where the blast load was simulated using Lagrangian–Eulerian domain coupling. The developed method proved to be a very efficient way to assess the load carrying capacity of a column with imperfections caused by dynamic, blast loading. The results of analyses indicated that the column (HKS-300 cross-section) is very resistant to blast loading. High deformation of its structure (close to ultimate strains) caused only 10% reduction of the load carrying capacity. Separation between a web and flanges of the I-column was the only factor that caused the significant loss of carrying capacity. Moreover, not only the mass of a charge influences the structural behaviour but also the explosive shape as well as the initiation point of detonation can significantly change the level of structure damage. Initiation point of detonation at the back of HE heavily increased blast pressure during interaction with the structure and a cylindrical shape of the explosive also increased the energy absorbed by the column. On the other hand, the use of the spherical charge or frontal detonation significantly reduced the destructive capabilities of the explosives.



## 1. Introduction

Nowadays, a high risk of terrorist attacks is observed. Bombing attacks are the most frequent terrorist activities [1,2]. Unfortunately, public infrastructure such as airports and railway stations, shopping centres, offices, financial and government institutions are highly exposed to such attacks. There were also several cases of such attacks with thousands of victims in Europe (Madrid 2004 and London 2005) [3,4]. Blast loading of the critical supporting elements of public facilities can cause considerable reduction of its carrying capacities, as well as partial or global collapse of the building. Progressive collapse took place during Oklahoma City bombing, where 87% of deaths were caused not by the direct effects of the blast overpressure but by the subsequent collapse of a significant part of the building, as a result of the reduced load-carrying capacity of the structural system [5].

The problem of blast wave interaction with a structure and its destructive effect has been already presented in many papers [6–11]. In the numerical studies of blast wave interaction with structures, Finite Element Method (FEM) is the most common approach to assess the structure response. Two main types of methods of blast loading numerical simulation can be distinguished: the application of pressure loading, such as Conwep [12,13] and the description of detonation, blast wave propagation in fluid domain and fluid structure interaction, e.g. Computational Fluid Dynamic methods (CFD) or Multi Material Arbitrary Lagrangian Eulerian formulation (MM-ALE) [14,15]. It is also possible to assess the structure response caused by the blast wave using simple methods, namely, single or multi degree of freedom methods [16,17]. Comparison of these groups of analyses methods and several algorithms of structure dynamic loading were presented in the authors' previous study [18].

The authors' previous research proved that dynamic response and deformations of the structural elements due to blast impact can be accurately predicted [19]. Nevertheless, dynamic response of the analysed element is insufficient to assess the structure stability. It was found that the residual load carrying capacity of the supporting elements is critical for global stability as well as safety of the occupants. Determination of the ultimate axial load for the supporting structures, also with imperfections, is a very common problem and can be easily solved using both numerical

* Corresponding author.
*E-mail addresses:* lmazurkiewicz@wat.edu.pl (L. Mazurkiewicz), jerzy.malachowski@wat.edu.pl (J. Malachowski), pbaranowski@wat.edu.pl (P. Baranowski).

http://dx.doi.org/10.1016/j.engstruct.2015.09.025
0141-0296/

and analytical methods [20–22]. However, it should be noticed that those procedures usually do not take into consideration the residual stress state after the blast, but only the geometrical imperfections (deformation). The main object of the paper is to demonstrate the efficiency and effectiveness of the proposed advanced multistage analysis procedure for the analysis of a supporting structure load capacity. Various authors present a similar approach in [23–26], however, the procedures were very time consuming due to the use of only an explicit code in all stages. In the presented method, a numerical algorithm switches from an implicit to explicit scheme (and vice versa) in order to take advantages of each method, such as efficient quasi-static solution using an implicit scheme and capability to solve highly dynamic blast loading phenomena using an explicit code.

## 2. Analysed problem

In the performed studies the blast resistance of a steel supporting column was analysed. Geometry of the analysed structure is shown in Fig. 1(a). The I-column (HKS-300 cross-section) has web thickness of 10 mm, flanges thickness of 20 mm and web and flanges width of 300 mm. On its upper surface/edge, there was applied a load simulating the weight of a roof surrounding structure, represented by force $P_n$ and lumped mass $M_n$. Mass of the detonated 4-kilo high explosive (HE) was evaluated based on the "abandoned briefcase" scenario, in which a briefcase filled with TNT is placed near the column (Fig. 1(b)). The charge standoff distance measured from the web face was 550 mm and the height measured from the charge lower edge to the floor was 200 mm. From the analytical point of view, such a scenario means that blast wave interacts with a preloaded I-column. Therefore, the static stages (preload and ultimate load investigation) have to be separated by highly dynamic stage (blast loading), which must be analysed using special numerical methods.

Evaluation of a blast influence on the load capacity of the investigated structure was carried out by comparing the results derived from the following set of cases:

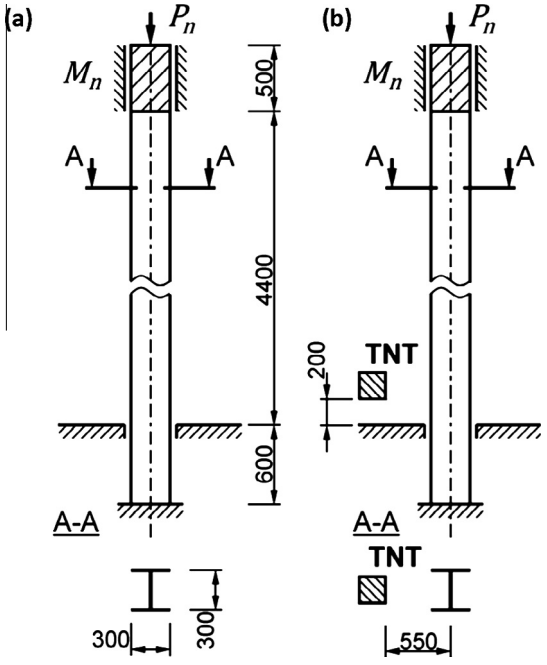


**Fig. 1.** Object of interest – I-column (a) case without deformations and (b) case with blast loading from TNT charge (mm).

- reference I-column structure (undeformed),
- column subjected to blast wave generated by TNT charges with constant 550 mm standoff distance and:
  - different masses: 2 kg, 4 kg, 6 kg (cubical charge, centre point of detonation),
  - different shapes: spherical, cubic and cylindrical with diameter to height ratio equal to 3 (mass 6 kg and centre point of detonation),
  - different initiation points of detonation: front, centre, rear (cubical charge, mass 4 kg).

## 3. Numerical model development

A discrete model of the steel column was developed using 8-node thick shell elements, which, in fact, are brick elements but with thick shell and co-rotational formulations introduced [27]. A connection of the column to a concrete foundation was modelled by fixing translational degrees of freedom of nodes corresponding to the place where the column is bolted (Fig. 2). Additional rigid walls were also introduced to describe contact conditions between the concrete base and the structure (Fig. 2). The full FE model consisted of 188 000 Lagrange (structural) elements.

The elastic–plastic material model with isotropic hardening including a strain rate effect was applied to describe the steel elements properties. The Johnson–Cook (JC) model provides a satisfactory prediction of flow stress $\sigma_{flow}$ for large strains and high strain rates when its dependence on strain rate is linear in a semi-logarithmic scale. The mathematical formula which describes this model is as follows [27,28]:

$$\sigma_{flow} = [A + B(\varepsilon^p)^n](1 + C \ln \dot{\varepsilon}^p_*)\left[1 - \left(\frac{T - T_{room}}{T_{melt} - T_{room}}\right)^m\right] \quad (1)$$

where $A$, $B$, $C$, $n$, $m$ – material constants and $\dot{\varepsilon}^p_*$ – effective plastic strain rate, $T$ – actual temperature based on plastic work, $T_{room}$ – room temperature, $T_{melt}$ – melting temperature. The required material properties were taken from a static tensile tests and dynamic tests (split Hopkinson pressure bar (SHPB) test [29,30]) carried out using the samples obtained from I-column material (Table 1).

The analysis performed by the authors indicated that the growth of temperature produced by plastic deformation while validating the current model was less than 100 °C. At this temperature, an influence of temperature on the yield stress of steel is very low [31], therefore, a thermal part in the JC equation was omitted. Tests results (see Section 5) also showed no influence of temperature on the web fracture edges.

The strain at fracture is given by equation:

$$e_f = [D_1 + D_2 e^{D_3 p/\sigma_{eff}}](1 + D_4 \ln \dot{\varepsilon}^p_*)\left[1 - D_5\left(\frac{T - T_{room}}{T_{melt} - T_{room}}\right)\right] \quad (2)$$

where $D_1$, $D_2$, $D_3$, $D_4$ and $D_5$ – material constants, $p$ – pressure, $\sigma_{eff}$ – effective stress. In the presented analysis, only $D_1$ parameter equals to 0.24 was used, which resulted from insufficient material data available. Parameters $D_2$–$D_5$ were assumed to be zero. Additionally, a strain limit in the welding areas was reduced by 30% [32].

## 4. Multistage numerical procedure

The authors decided to use commercial solver LS-Dyna [26], which is suitable for the analysis of high speed phenomena. The major advantage of this choice is a capability to link different types of solvers implemented within the frame of one numerical code. In the presented study, a multistage numerical analysis procedure was used to consider a full load path in residual load capacity

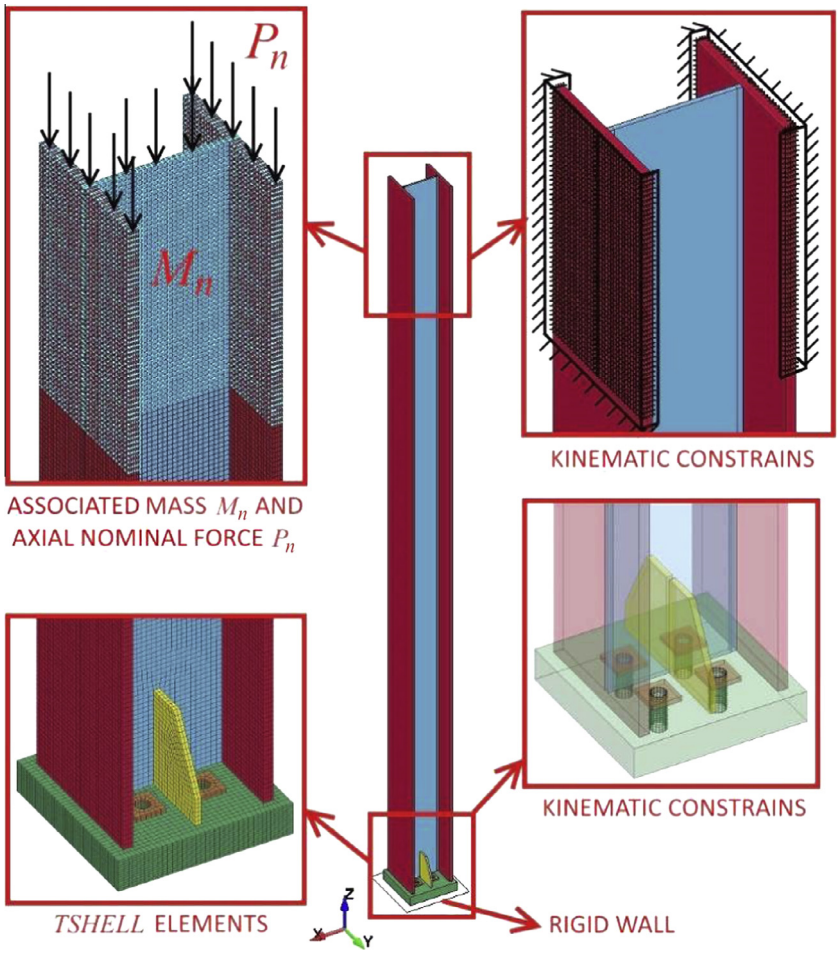


**Fig. 2.** Discrete model of I-column and boundary conditions.

**Table 1**
Material properties for S235JR steel (1.0037, AISI 1015) where: $\rho$ – density, $E$ – Young modulus, $\nu$ – Poisson ratio.

| $\rho$ (kg/m$^3$) | $E$ (GPa) | $\nu$ (–) | $A$ (MPa) | $B$ (MPa) | $C$ (–) | $n$ (–) | $D_1$ (–) |
|---|---|---|---|---|---|---|---|
| 7850 | 200 | 0.28 | 263 | 550 | 0.02 | 0.5 | 0.24 |

assessment. The following steps have been taken into account (Fig. 3): static preload (stage 1), dynamic blast loading with fluid structure interaction (FSI) (stage 2), dynamic response after blast loading (stage 3) and a static load carrying capacity assessment (stage 4). The investigation of the undeformed structure was performed with a single static step consisting of preload and assessment of ultimate axial force.

### 4.1. The first stage – preload

In the first stage, the I-column structure was subjected to service load $P_n$ = 1569.5 kN, equal to the load supported by the column under the designed conditions. Incremental static analysis was performed using a full Newton–Raphson algorithm. The equation solved in this stage has the following form [26]:

$$K_n \Delta x_{n+1} = F^{ext}_{n+1} - F^{int}_n \tag{3}$$

where $K_n$ – tangent stiffness matrix, $\Delta x_{n+1}$ – increment in displacement vector, $F^{ext}_{n+1}$ – external and body force loads, $F^{int}_n$ – the stress divergence vector.

Convergence of the solution was controlled by two criteria: displacement relative convergence tolerance $\varepsilon_{disp} = \|\Delta x^i\| / \Delta x_{max} = 0.001$ and energy relative convergence tolerance $\varepsilon_{energ} = |\Delta x^i Q^i| / |\Delta x^0 Q^0| = 0.01$, where $Q^i = F^{ext}_i - F^{int}_i$ and $i$ – implicit solver iteration. As a result of this stage, uniform stress distribution was obtained (except areas with constrains applied). Due to usage of the implicit solver, the computation time was reduced to ~20 min on 6 core PC.

### 4.2. The second stage – blast loading

In the second stage, the results from the previous stage were taken into account as a pre-stress field distributed in the column, which was accomplished using a stress initialization procedure between the stages. The blast loading in this stage required to switch to a transient dynamics procedure with explicit central difference time integration. In this case, the equation solved has the following form [26]

$$M\ddot{x}_n = F^{ext}_n - F^{int}_n - C\dot{x}_n \tag{4}$$

where $M$ – the diagonal mass matrix, $F^{ext}_n$ – external and body force loads, $F^{int}_n$ – the stress divergence vector, $C$ – damping matrix based on Rayleigh damping coefficients.

For the blast loading stage, over 904 000 Euler (fluid) elements were introduced into the numerical model. Some additional elements were implemented to describe the volume of gases

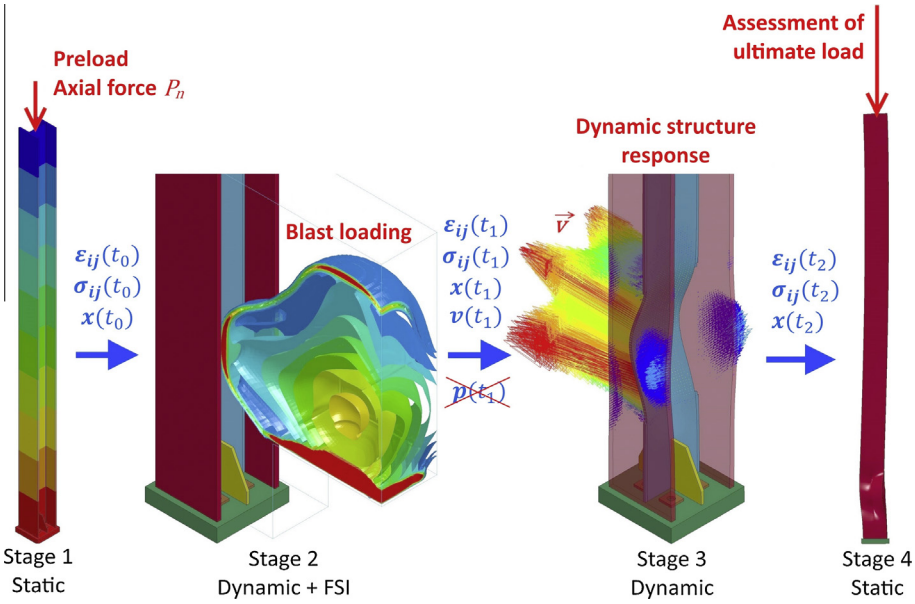


**Fig. 3.** Scheme of developed numerical procedure, where $\varepsilon_{ij}$, $\sigma_{ij}$ – strain and stress tensors; $x$, $v$ – displacement and velocity vectors, $p$ – pressure from blast loading vector; $t_0$, $t_1$, $t_2$ – moments in time after stage 1, 2 and 3.

**Table 2**
Material properties for HE.

| $\rho_{HE}$ (kg/m$^3$) | $D$ (m/s) | $P_{CJ}$ (GPa) | $A_{HE}$ (GPa) | $B_{HE}$ (GPa) | $R_1$ (–) | $R_2$ (–) | $\omega$ (–) | $\bar{e}_0$ (J/mm$^3$) |
|---|---|---|---|---|---|---|---|---|
| 1630 | 6930 | 21 | 371.2 | 3.230 | 4.15 | 0.95 | 0.3 | 7 |

surrounding the column. The blast wave generation was simulated by describing the behaviour of a highly compressed detonation product after reaching the successive locations by the detonation wave front. The Jones Wilkins Lee (JWL) equation of state was used in the following form [26]:

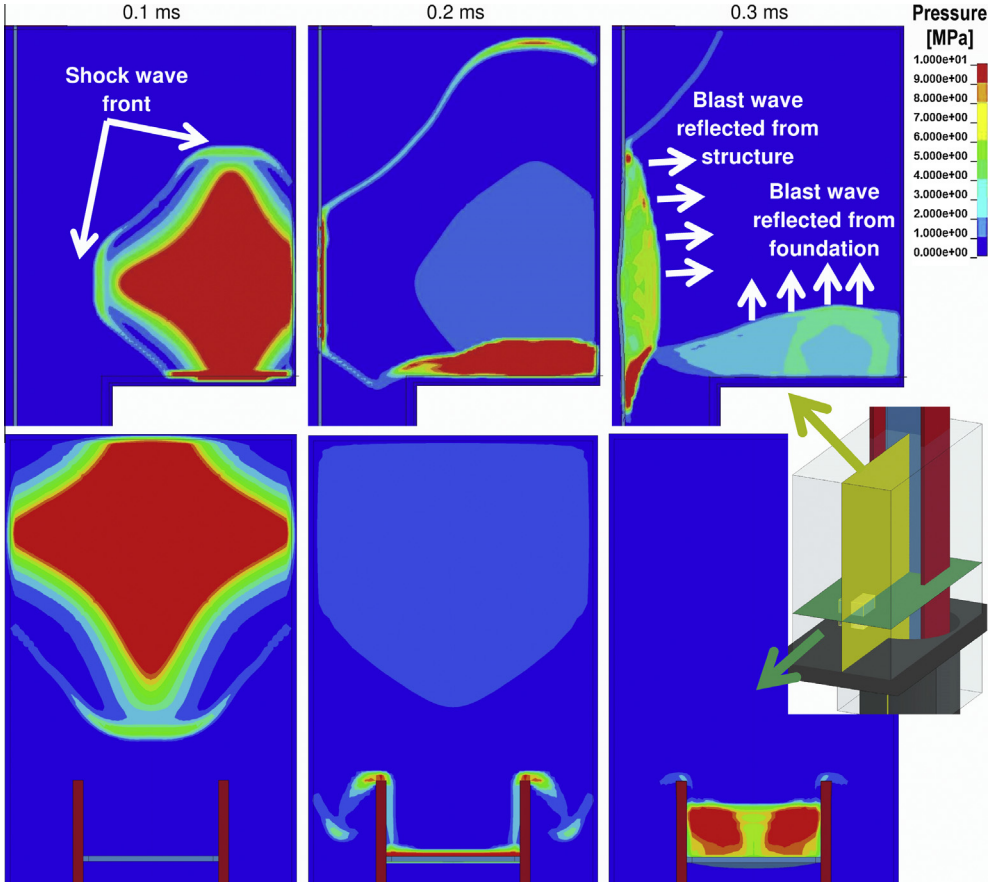


**Fig. 4.** Blast wave propagation and interaction with structure: vertical (yellow plane) and horizontal (green plane) cross sections (4 kg cubical TNT charge, centre detonation, 550 mm standoff distance). (For interpretation of the references to colour in this figure legend, the reader is referred to the web version of this article.)

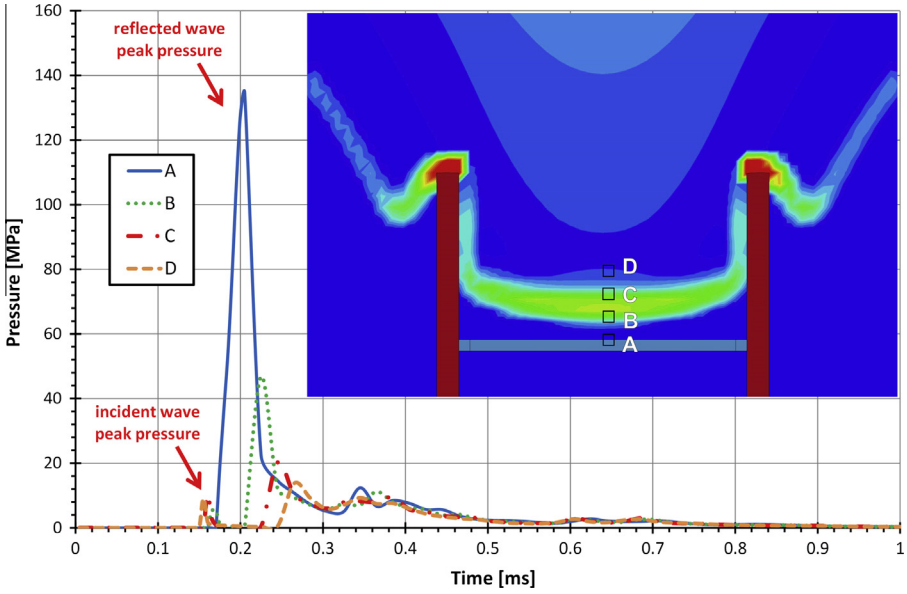


**Fig. 5.** Pressure characteristics within I-column area (4 kg cubical TNT charge, centre detonation, 550 mm standoff).

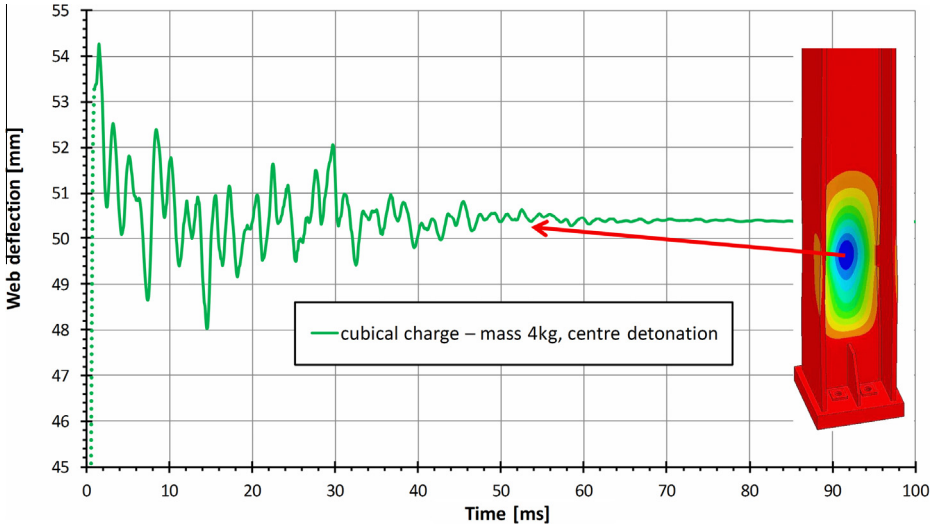


**Fig. 6.** Web deflection of beam-column subjected to 4 kg cubical TNT charge (centre detonation, 550 mm standoff).

$$p = A_{HE}\left(1 - \frac{\omega}{R_1\overline{\rho}}\right)\exp(-R_1\overline{\rho}) + B_{HE}\left(1 - \frac{\omega}{R_2\overline{\rho}}\right)\exp(-R_2\overline{\rho}) + \frac{\omega\overline{e}}{\overline{\rho}} \tag{5}$$

where $\overline{\rho} = \rho_{HE}/\rho_{DET}$; $\overline{e} = \rho_{HE}e$; $\rho_{HE}$ – density of high explosive, $p$ – pressure; $e$ – specific internal energy, $\rho_{DET}$ – density of detonation product. $A_{HE}$, $B_{HE}$, $R_1$, $R_2$, $\omega$ – empirical constants determined for a specific type of explosive. All the required constants were taken from literature [33] (Table 2).

The blast propagation was accomplished using MM-ALE procedure involving two steps: a classical Lagrangian step and an advection step, with the following sub-steps included: relocation of the nodes, recalculation of all variables as referred to the elements and reevaluation of the momentum and velocity updating. The advection step is carried out under the assumption that the changes in positioning of the nodes are negligible in comparison to the element size. The interaction between the propagating blast wave and the structure was obtained by adopting a coupling algorithm between the Euler (product of detonation) and the Lagrange (steel structure) domains based on the penalty function method [34].

In the performed simulations, the generated shock waves interact with the I-column and deform the structure. In the pressure maps (Fig. 4), the shock wave front and the wave reflected from the I-column and as well as foundation can be clearly seen.

It should be also pointed out that, due to section shape (flanges are flow boundaries), a reflected to incident peak pressure ratio was very high compared to a plain surface ratio (Fig. 5).

Due to introduction of a number of the fluid domain elements as well as FSI interface, the computational cost significantly increased. The phenomenon duration simulated in the analysis in this stage has been reduced to 1 ms. After this time the fluid interaction is negligible (see Fig. 5). The total time of calculations for this case was about 10 h.

### 4.3. The third stage – dynamic structure response

In the following stage, dynamic I-column response after the blast wave interaction was assessed. The main difference from the previous stage was that the focus of analysis was the column without fluid. Therefore, the Eulerian domain together with corre-

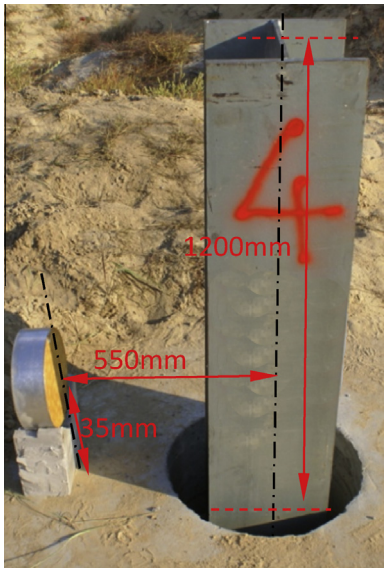


**Fig. 7.** Experimental set-up.

sponding FSI interface were removed from the numerical model. This allowed for reducing the FE model to the previous size (188 000 elements – almost 6 times less than in the full model) and thus, to increase the simulation time in the analysis from 1 ms to 100 ms and to reduce the total analysis time required for computations to 5 h. During the last 50 ms of the analysis, the damping coefficient was increased in order to effectively reduce the magnitude of oscillations (Fig. 6).

### *4.4. The fourth stage – assessment of ultimate load*

The final stage was similar to the first one. As in the case of the first stage, a static analysis with Newton–Raphson procedure was involved. The convergence was based on relative displacement tolerance ($\varepsilon_{disp} = 0.001$) and energy tolerance ($\varepsilon_{disp} = 0.01$) with a minimum allowed load step equal to 0.001 of the service axial load $P_n$. The structure was loaded by a multiple of the service load $P_n$, so that the iteration procedure could reach the point of divergence, which resulted from an ill-conditioned stiffness matrix. A load value causing divergence conditions was considered as the load capacity of the structure. It should be pointed out that, due to the chosen algorithm (Newton–Raphson), this is the approximate value of the ultimate force. The computational time for this stage was about 1 h, which was considerably shorter than in the case of explicit stages.

## 5. Experimental validation

In order to validate the numerical model, the experimental test was performed. The beam-column was subjected to a pressure wave from the cylindrical charge with the mass of 6 kg. Moreover, to simplify the test, the I-beam length was reduced to 1565 mm and the axial load was not taken into consideration (Fig. 7). In the numerical computations carried out to validate the model, only two stages were performed: the dynamic impact of gaseous medium (blast wave) and further dynamic response of the structure. No preload and load carrying assessment were needed.

The results from both numerical simulation and experimental tests are presented in Figs. 8 and 9. It can be noticed that the obtained levels of damage are comparable. In the authors' opinion, this model can be considered as partially validated for simulation of the detonation process, blast wave propagation and its interaction with the structure. The proposed discrete model, including the applied material models and equations of state, yields good agreement with the test data.

Moreover, in the field test no temperature effects such as melting of the I-column edges were observed.

## 6. Results

The multistage analyses were performed for different HE masses, shapes and initiation points of detonation. As expected, an influence of the first parameter – the mass, is very significant. The explosive charges with masses of 2 kg, 4 kg and 6 kg generate shock waves with considerably different pressures. As a result of the blast wave interaction with the structure, high plastic deformations were obtained. For the case with the mass 4 kg, a small frac-

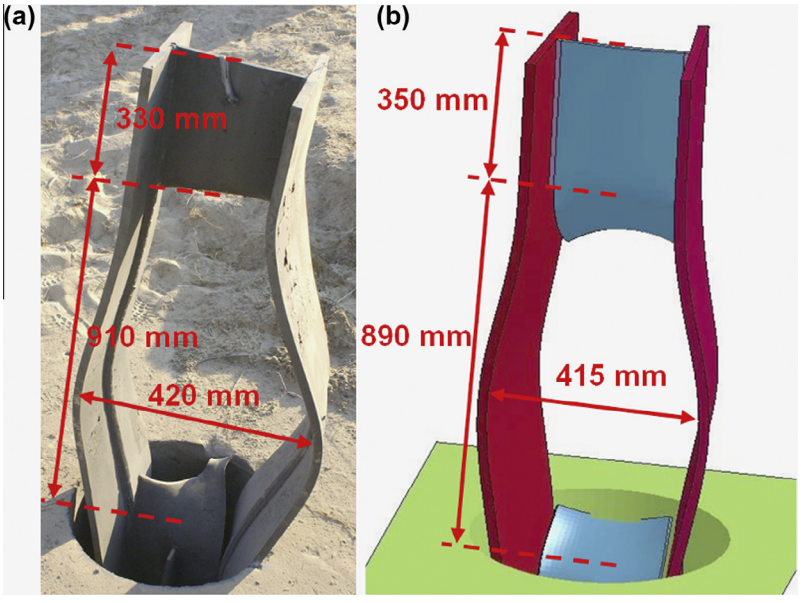


**Fig. 8.** Destruction of I-beam – (a) experimental and (b) numerical results – front view (6 kg cylindrical TNT charge, 550 mm standoff distance).

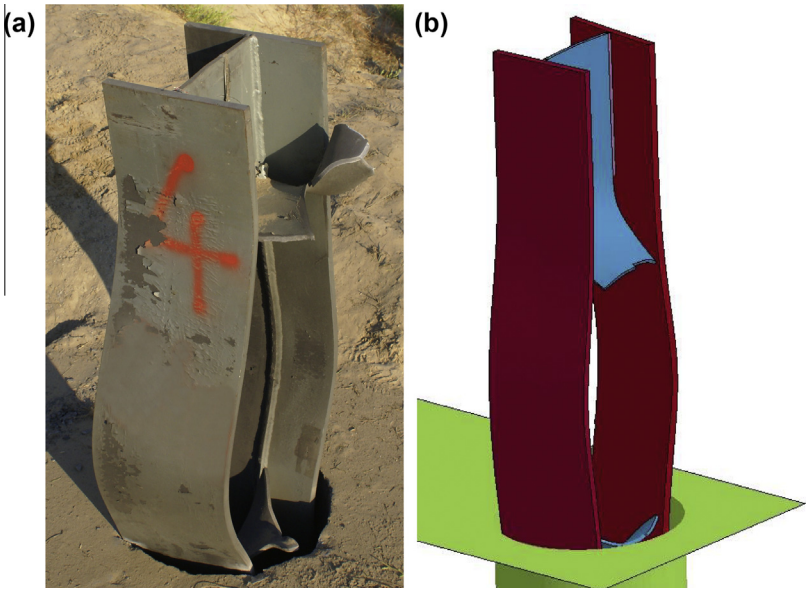


**Fig. 9.** Destruction of I-beam – (a) experimental and (b) numerical results – side view (6 kg cylindrical TNT charge, 550 mm standoff distance).

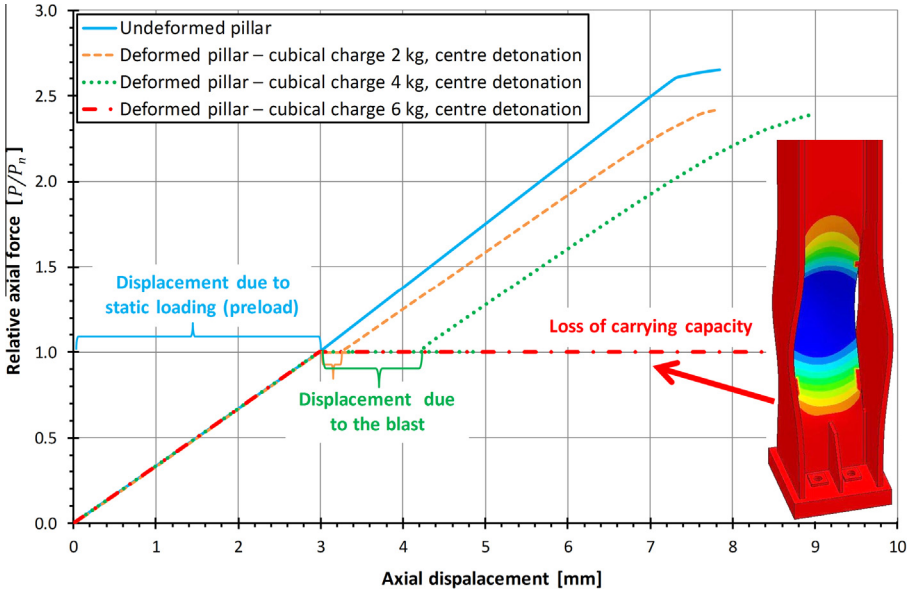


**Fig. 10.** Influence of charge mass on residual carrying capacity (cubical charge, centre point of detonation, 550 mm standoff).

ture (70 mm long) in the area of the web and flanges connection occurred; however, the detonation of the 6 kg charge caused heavy damage to the I-column. The significant separation of the web and flanges resulted in a loss of the load carrying capacity below the service load and dynamic destruction. On the other hand, for the two cases with a lower charge mass, reduction of the carrying capacity was less than 10% (Fig. 10).

During the investigation, it was found that the shape of HE also significantly affected the results. An pressure averaged over an area was derived, as more suitable for comparison purposes. For the mass of 6 kg, the cubical charge generates a blast wave with a peak pressure almost 8 times higher than the peak pressure from the spherical charge (Fig. 11). Moreover, the cylindrical charge generated even 10 times higher pressure. In this case, the blast wave interaction resulted in very high deformations and separation of a large part of the I-column web. The load carrying capacity was almost completely eliminated (Fig. 12), whereas the relatively low pressure (few times lower) from the spherical charge causes only 10% of the load carrying capacity reduction.

Coupling blast pressure is also dependent on the location of the initiation point of detonation. The results of the analysis indicates that the shift of the initiation point at the back of HE (further from the structure) increased an coupling pressure (about 20% in studied conditions) and the detonation at the front of the charge decreased the pressure almost 4 times. It was also reflected in the beam-column response (deformation) and its reduction of the carrying capacity. For the case with the rear detonation point, the ultimate force was reduced by 30% (Fig. 13).

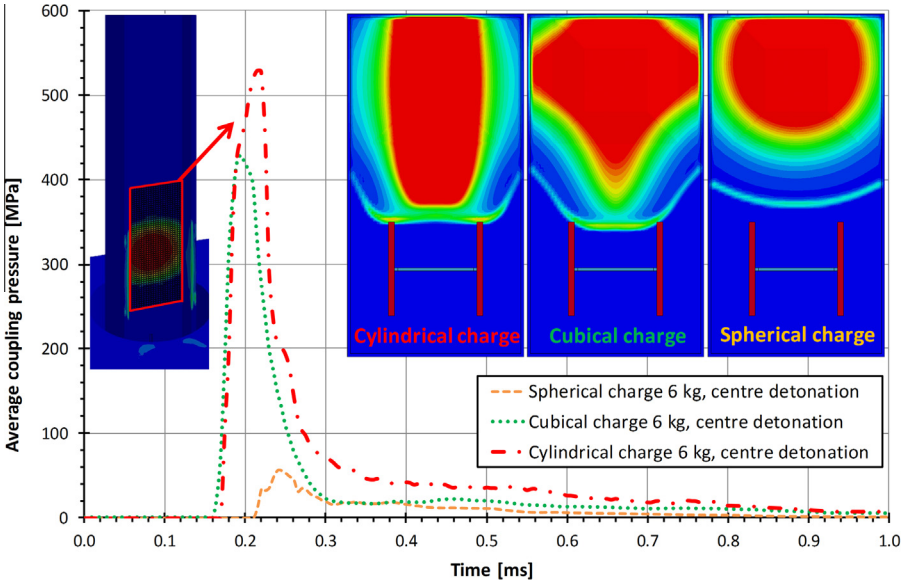


**Fig. 11.** Pressure characteristics within I-column area for different charge shapes (6 kg TNT charge, centre detonation).

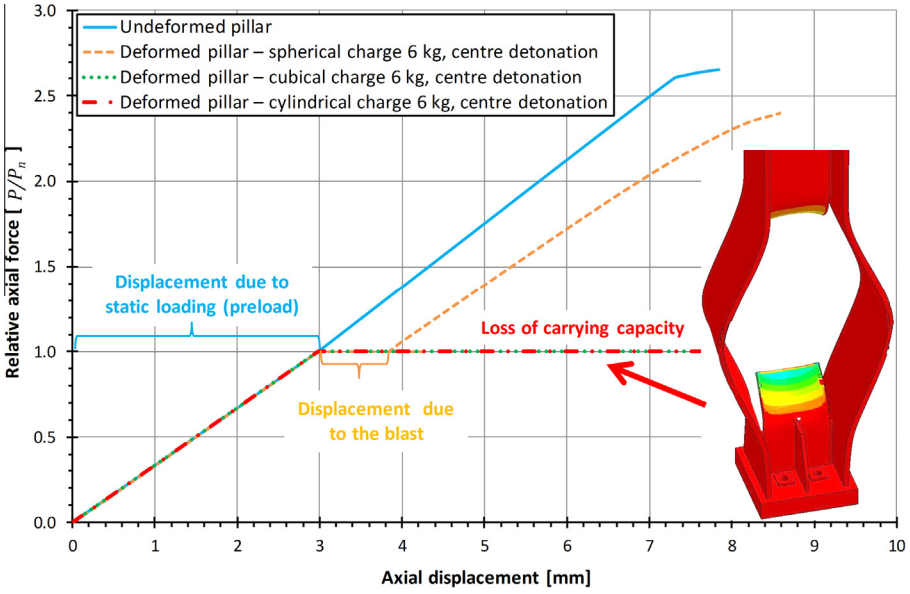


**Fig. 12.** Influence of charge shape on residual carrying capacity (6 kg TNT charge, centre detonation).

## 7. Conclusions

The paper demonstrates the advantages of the proposed multi-stage analysis procedure for the load carrying capacity assessment. From a numerical point of view, the developed analysis path consists of two different solution algorithms: implicit and explicit schemes.

The stress initialization option allows introduction of the stress and strain field from previous stage to analysis with different conditions and solution algorithms. Finally, a full load path i.e., pre-load, blast loading, dynamic response and ultimate load assessment can be simulated using one model in relatively low CPU time (below 17 h using PC with 6 core 4 GHz CPU and a double precision solver).

The performed simulations clearly showed that a relatively small explosive charge can cause high-deformation of the I-column. Due to a section shape (flanges are flow boundaries), a reflected to incident peak pressure ratio was very high compared to a plain surface ratio. It should be also pointed out that the developed numerical model was partially validated by the field tests. The developed discrete model with the applied material models and equations of state provides good agreement with the test results.

Evaluation of the blast influence on the load capacity of the investigated structure was carried out by comparing the results derived from the cases with different explosive mass, location of the initiation point and shape. The results show that not only the mass of the detonated charge influences the structure behaviour but also its shape and the initiation point of detonation, which can significantly change the extent of the structure damage. Initiation at the back of HE heavily increased the average coupling pressure during interaction with the structure and a cylindrical

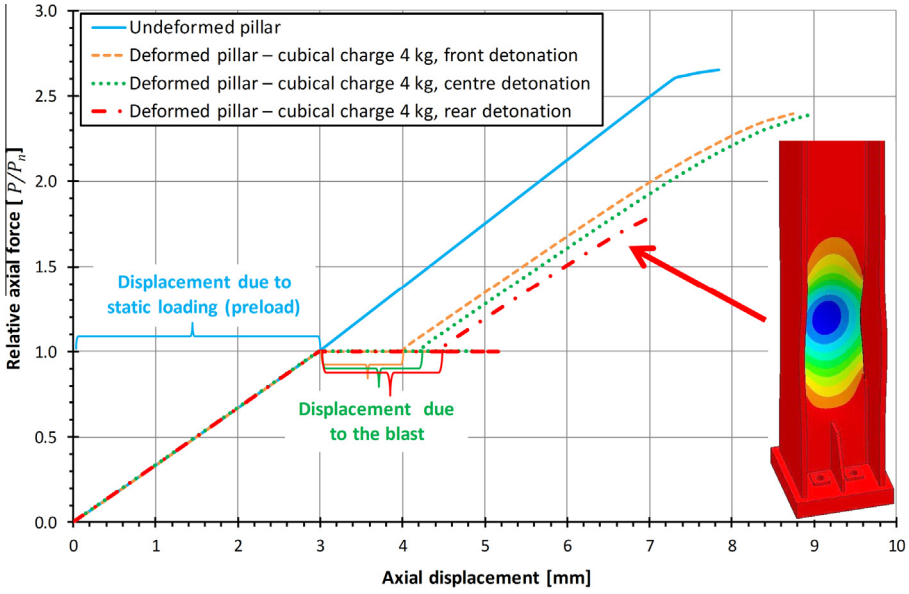


**Fig. 13.** Influence of initiation point of detonation on residual carrying capacity (4 kg TNT cubical charge).

shape of the explosive also increased the energy absorbed by the column. On the other hand, the use of the spherical charge or frontal detonation greatly reduced the destructive capabilities of the explosives. Moreover, the I-column used in this research was very resistant. High deformation of its structure (close to ultimate strain equal to 0.24 and 0.17 for the welds) caused only 10% reduction of the load carrying capacity. Separation between the web and the flanges was the only factor that resulted in a significant loss of the carrying capacity.

The authors' further investigations will be focused on development of the optimised blast protective panel for the supporting elements.

## Acknowledgements

The research was carried out under a research grant from Polish Ministry of Science and Higher Education no. 0097/R/T00/2010/12. This support is gratefully acknowledged.

## References

[1] Global Terrorism Database (GTD); 2011. <http://www.start.umd.edu/gtd/features/GTD-Data-Rivers.aspx>.
[2] Worldwide Incidents Tracking Systems. National Counterterrorism Center (NCTC). <https://wits.nctc.gov>.
[3] Martí M, Parrón M, Baudraxler F, Royo A, Gómez León N, Álvarez-Sala R. Blast injuries from Madrid terrorist bombing attacks on March 11, 2004. Emerg Radiol 2006;13:113–22.
[4] Strom KJ, Eyerman J. Interagency coordination: lessons learned from the 2005 London train bombings. NIJ J 2005;2008:260.
[5] Site and Urban Design for Security. Guidance against potential terrorist attacks. US Federal Emergency Management Agency; 2007.
[6] Tang E, Hao H. Numerical simulation of a cable-stayed bridge response to blast, loads, Part I: Model development and response calculations. Eng Struct 2010;32:3180–92.
[7] Lu Y, Wang Z. Characterization of structural effects from above-ground explosion using coupled numerical simulation. Compos Struct 2006;84:1729–42.
[8] Chafi MS, Karami G, Ziejewski M. Numerical analysis of blast-induced wave propagation using FSI and ALE multi-material formulations. Int J Impact Eng 2009;36(10):1269–75.
[9] Morka A, Kwasniewski L, Wekezer JW. Assessment of passenger security in paratransit buses. J Public Transport 2005;8(4):47–63.
[10] Williams K, McClennan S, Durocher R, St-Jean B, Joccelyn T. Validation of a loading model for simulating blast mine effects on armoured vehicles. In: Proceedings of the 7th international LS-DYNA users conference, Salzburg; 2002. p. 35–44.
[11] Li J, Rong J. Experimental and numerical investigation of the dynamic response of structures subjected to underwater explosion. Eur J Mech B. Fluids 2010;32:59–69.
[12] CONWEP. Conventional Weapons Effects, US Army TM-855; 1992.
[13] Randers-Pehrson G, Bannister KA. Airblast loading model for DYNA2D and DYNA3D ARL-TR-1310. Adelphi MD: Laboratory AR., Ed. USA; 1997.
[14] Benson DJ. Computational methods in Lagrangian and Eulerian hydrocodes. Comput Methods Appl Mech Eng 1992;99:235–394.
[15] Belytschko T, Liu WK, Moran B. Nonlinear finite elements for continua and structures. England: John Wiley & Sons; 2000.
[16] Nassr AA, Razaqpur AG, Tait MJ, Campidelli M, Foo S. Single and multi degree of freedom analysis of steel beams under blast loading. Nucl Eng Des 2012;242:63–77.
[17] User Guide for the Single degree of freedom Blast Effects Design Spreadsheet (SBEDS). US Army Corps of Engineers; 2008.
[18] Mazurkiewicz L, Malachowski J, Baranowski P, Damaziak K. Comparison of numerical testing methods in terms of impulse loading applied to structural elements. J Theor Appl Mech 2013;51:615–25.
[19] Malachowski J. Influence of HE location on elastic–plastic tube response under blast loading. Shell Struct Theor Appl 2010;2:179–82.
[20] Gurel MA, Pekgokgoz RK, Cili F. Strength capacity of unreinforced masonry cylindrical columns under seismic transverse forces. Bull Earthquake Eng 2012;10:587–613.
[21] Machado S. Non-linear stability analysis of imperfect thin-walled composite beams. Int J Non Linear Mech 2010;45:100–10.
[22] Liu Y, Gannon L. Finite element study of steel beams reinforced while under load. Eng Struct 2009;31(11):2630–42.
[23] Wu K, Li B, Tsai K. The effects of explosive mass ratio on residual compressive capacity of contact blast damaged composite columns. J Constr Steel Res 2011;67:602–12.
[24] Bao X, Li B. Residual strength of blast damaged reinforced concrete columns. Int J Impact Eng 2010;37:295–308.
[25] Jayasooriya R, Thambiratnam DP, Perera NJ, Kosse V. Blast and residual capacity analysis of reinforced concrete framed buildings. Eng Struct 2011;33:3483–95.
[26] Ding Y, Wang M, Li XZ, Hao H. Damage evaluation of the steel tubular column subjected to explosion and post-explosion fire condition. Eng Struct 2013;55:44–55.
[27] Hallquist JO. LS-Dyna Theory manual. Livermore. California; 2006.
[28] Johnson GJ, Cook WH. A constitutive model and data for metals subjected to large strains, high strain rates and high temperatures. In: Proceedings of the seventh international symposium on ballistics, The Hague; 1983. p. 541–7.
[29] Gray GT. Classic split-Hopkinson pressure bar testing, mechanical testing and evaluation. Metals handbook, vol. 8; 2000. p. 462–76.
[30] Baranowski P, Gieleta R, Malachowski J, Damaziak K, Mazurkiewicz L. Split Hopkinson pressure bar impulse experimental measurement with numerical validation. Metrol Meas Syst 2014;21(1).
[31] Mocko W, Kruszka L. Results of strain rate and temperature on mechanical properties of selected structural steels. Procedia Eng 2013;57:789–97.
[32] Design of steel structures – Part 1–8: Design of joints, BS EN 1993-1-8; 2005.
[33] Wlodarczyk E. Fundamentals of detonation. Warsaw: Military University of Technology; 1995.
[34] Haufe A, Weimar K. Proceedings of the 5th European LS-DYNA users conference, Birmingham; 2005. p. 5c-59.